International Journal of Heat and Mass Transfer 54 (2011) 2154–2162

Contents lists available at ScienceDirect

International Journal of Heat and Mass Transfer

journal homepage: www.elsevier.com/locate/ijhmt

Investigation of heat transfer and pressure drop of CO_2 two-phase flow in a horizontal minichannel

J. Wu [a], T. Koettig [a], Ch. Franke [b], D. Helmer [a], T. Eisel [a], F. Haug [a], J. Bremer [a,*]

[a] CERN, TE-CRG-CI, 1211 Geneva 23, Switzerland
[b] University of Applied Science, Esslingen, Germany

ARTICLE INFO

Article history:
Received 30 August 2010
Received in revised form 24 November 2010
Available online 17 January 2011

Keywords:
Heat transfer
Pressure drop
Heat flux
Mass flux
Saturation temperature
Predication model
CO_2

ABSTRACT

An innovative cooling system based on evaporative CO_2 two-phase flow is under investigation for the tracker detectors upgrade at CERN (European Organization for Nuclear Research). The radiation hardness and the excellent thermodynamic properties emphasize carbon dioxide as a cooling agent in the foreseen minichannels. A circular stainless steel tube in horizontal orientation with an inner diameter of 1.42 mm and a length of 0.3 m has been used as a test section to perform the step-wise scanning of the vapor quality in the entire two-phase region. To characterize the heat transfer and the pressure drop depending on the vapor quality in the tube, measurements have been performed by varying the mass flux from 300 to 600 kg/m^2 s, the heat flux from 7.5 to 29.8 kW/m^2 and the saturation temperature from −40 to 0 °C (reduced pressures from 0.136 to 0.472). Heat transfer coefficients between 4 kW/m^2 K and 28 kW/m^2 K and pressure gradients up to 75 kPa/m were registered. The measured data was analyzed corresponding to the dependencies on heat flux, mass flux and saturation temperature. A database has been established containing about 2000 measurement points. The experimental data was compared with common models recently developed by Cheng et al. [1,2] to cross check their applicability. The overall trends and experimental data were reproduced as predicted by the models before the dryout onset, and deviations have been analyzed. A modified friction factor for the pressure drop model [1] in mist flow has been proposed based on the experimental data.

1. Introduction

After several years of running the Large Hadron Collider (LHC), CERN will upgrade to the super LHC (sLHC) increasing the luminosity by a factor of 10 to allow new physics discoveries and to open a new physics field [3,4]. The corresponding upgrade of the Compact Muon Solenoid experiment (CMS) foresees a heat dissipation of 144 W along a 5.5 m long circular cooling tube with an inner diameter of 1.42 mm [5,6].

CO_2 is classified as safe refrigerant and its Global Warming Potential is 1 by definition. The high latent heat of CO_2, the low pressure dependence of the temperature of the saturated liquid and the low viscosity help to design the heat exchanger tubes with small inner diameter and thus small wall thickness. Currently, a number of investigations on CO_2 are ongoing since it is one of the few natural refrigerants [7,8]. At NIKHEF a mechanically pumped CO_2 loop was developed for the cooling of the AMS (the Alpha Magnetic Spectrometer) Silicon Tracker [9]. The requirements of the cooling system for the LHCb-VErtex LOcator Experiment (VELO) at the CERN's Large Hadron Collider (LHC) have led to the use of CO_2 as evaporative cooling fluid [10]. CO_2 also appears to be a promising coolant for microprocessors at low operating temperatures [11].

These applications, the high latent heat, the low viscosity and the radiation hardness emphasize CO_2 as a potential substitute for C_6F_{14} (Perfluorohexane) presently used as refrigerant in the CMS pixel detector [5].

The presented measurements focus on the heat transfer coefficient and pressure drop in the CO_2 two-phase flow regime, in the range of relevant heat flux, saturation temperature and mass flux. The presented experimental data will contribute to the validation of the design rules and demonstrate the applicability of CO_2 cooling for CMS pixel detector upgrade.

In literature several experimental studies on heat transfer and pressure drop of CO_2 in minichannels are available [12–18]. The influences of mass flux, heat flux, vapor quality, and saturation temperature are presented in these publications. Published data related to CO_2 two-phase flow in minichannels are relatively few, compared to the data for macro-channels and for the conventional refrigerants, especially at high vapor qualities.

Many correlations have been proposed for the two-phase flow heat transfer [19–21] and pressure drop [22–24]. Flow pattern

* Corresponding author. Tel.: +41 22 76 78752; fax: +41 22 76 78885.
E-mail addresses: jihao.wu@cern.ch (J. Wu), torsten.koettig@cern.ch (T. Koettig), friedrich.haug@cern.ch (F. Haug), johan.bremer@cern.ch (J. Bremer).

0017-9310/$ - see front matter © 2010 Elsevier Ltd. All rights reserved.
doi:10.1016/j.ijheatmasstransfer.2010.12.009

Nomenclature

A	cross section (m^2)
D_h	hydraulic diameter (m)
f	friction factor
G	mass flux (kg/m^2 s)
h	enthalpy (kJ/kg)
$\dot{m}$	mass flow rate (kg/s)
$\bar{k}$	overall heat transfer coefficient (W/m^2 K)
Pr	Prandtl number
$\dot{q}$	heat flux (W/m^2)
r	radius (m)
R	thermal resistance (K/W)
Re	Reynolds number
Δp	pressure drop (kPa)
x	vapor quality
$\dot{Q}$	power (W)

Greek symbols

λ	thermal conductivity (W/m K)
$\dot{\alpha}$	mean heat transfer coefficient (W/m^2 K)
ω	flow velocity (m/s)

Subscripts

eff	effective
fl	fluid
in	inlet
out	outlet
l	liquid
v	vapor
start	start point
w	wall
w, i	inner wall
sat	saturation condition
PH	pre-heater
crit	critical
AH	after-heater
tr	thermal resistance
ts	test section

maps are very important to understand the very complex two-phase flow phenomena and heat transfer trends in flow boiling [25]. Cheng et al. [26] developed a new flow map and a new flow boiling heat transfer model for CO_2 evaporation. Furthermore, new data allowed an updated flow map, frictional pressure drop model and boiling heat transfer model for their new versions in 2008 [1,2].

The experimental results obtained in this study have been compared with these models. And maybe useful for further model improvements, as a large number of experimental data were obtained in this study especially at high vapor quality.

2. Experimental setup

The closed circuit of the CO_2 system is divided into a warm and a cold part as shown in Fig. 1. The setup is designed and tested for a maximum working pressure of 80 bar. The warm part consists of a CO_2 compressor (Danfoss® TN 1410), a homemade oil separator and filter unit, a mass flow meter, gas handling components and a reservoir. The cold part of the setup is installed inside a vacuum vessel which provides an insulation vacuum of 10^{-5} mbar. Additionally, the whole setup inside the vacuum vessel is surrounded by multi-layers insulation to significantly reduce the radiation heat transfer. The cold part is connected to the warm part via a concentric heat exchanger also located in the vacuum vessel. A Pulse Tube Refrigerator (PTR) is used as cold source, providing the cooling power to liquefy and sub-cool the CO_2 flow. The cold head temperature of the PTR can be controlled in a range from −60 to −10 °C. The condenser unit is subdivided into two reservoirs, where the upper one is filled with a copper mesh foreseen to liquefy the CO_2, while the lower part is in contact to the cold head of the PTR and operates as a sub-cooler for the CO_2.

Starting with sub-cooled liquid (see point 1 in Fig. 1) the two-phase region is entered by an isenthalpic expansion to point 2. This Joule–Thomson expansion is realized by an adjustable needle valve. The pre-heater applies heat to obtain a certain vapor quality at point 3. In addition with a heat input to the test section, a step-wise scanning of the whole vapor quality range at a constant saturation temperature is possible. The after-heater (AH) is regulated to assure that the total heating power of the pre-heater (PH), the test section (ts) and the AH maintained at a constant value. The aim is to keep a stable behavior of the whole thermodynamic cycle during the measurement.

3. Validation of the experimental setup

To perform a step-wise scanning of the two-phase region, a relative short test section is needed while taken into account the thermodynamic entry length [27]. The test section is made of a circular stainless steel tube. The inner diameter is identical to the foreseen heat exchanger tubes of the CMS inner tracker.

Fig. 2 illustrates the test section design to determine the heat transfer coefficient. The test section has a total length of 300 mm whereas the heated part l_{ts} is 150 mm long. A heat flux up to 29.8 kW/m^2 can be applied to the test section by a heating wire uniformly coiled around the tube. Three PT-100 temperature sensors are attached along the heated part via copper supports to measure the mean wall temperature $\overline{T}_w$.

To determine the mean fluid temperature $\overline{T}_{fl}$, two additional sensors are placed upstream and downstream of the test section at a defined distance l_{ts-fl} of 35 mm from the heated part. The temperature sensors are calibrated relatively to the fluid inlet temperature as measured by $T_{fl,in}$. Before the step-wise measurement procedure starts, this calibration is performed without heat input to the pre-heater and the test section at the appropriate temperature level. The precision of the temperature variation measurement is estimated to $\Delta T = \pm 0.05$ K.

The temperature gradient along the temperature measurement supports leads to an underestimation of the heat transfer coefficient. The effective thermal resistance of the temperature sensor support, which is basically a compound of thermal conductance grease, a thin solder layer and the bulk copper itself, can be assumed to be constant for the temperature interval of the measurement. An inverse overall heat transfer coefficient $1/\bar{k}$ valid for single-phase heat transfer derived from the single-phase heat transfer model from Gnielinski [28], can be written as:

$$\frac{1}{\bar{k}} = \frac{D_h}{\frac{(f/8)(Re-1000)Pr}{1+12.7\sqrt{(f/8)}(Pr^{2/3}-1)}\left[1+\left(\frac{D_h}{l}\right)^{(2/3)}\right]\left(\frac{Pr}{Pr_w}\right)^{0.11}\lambda} + R_{eff}A_{w,i} \quad (1)$$

where R_{eff} represents the effective thermal resistance of the temperature support compound. To determine R_{eff}, a set of measured single-phase heat transfer data points are plotted versus the

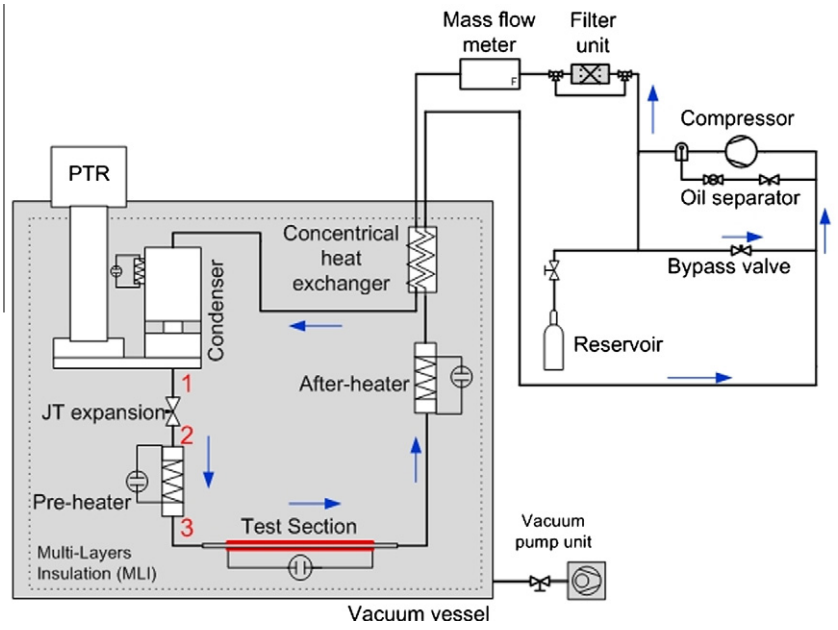

Fig. 1. Schematic of the experimental test setup. The measurement part is located in a vacuum chamber.

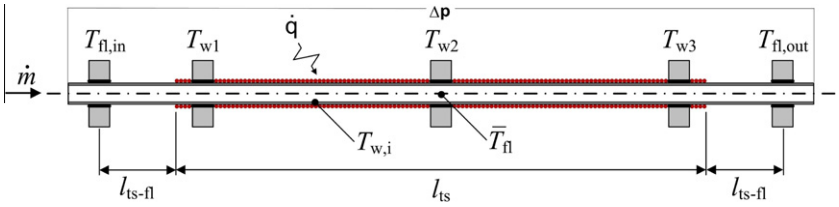

Fig. 2. Schematic of the test section with a total length of 300 mm including the heated part of 150 mm.

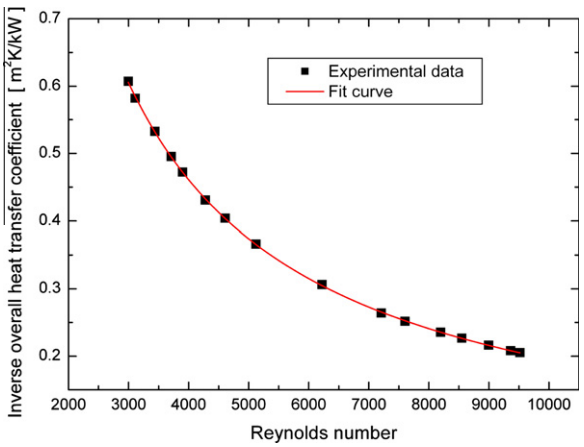

Fig. 3. Plot of the inverse overall heat transfer coefficient versus the Reynolds number to extrapolate the effective thermal resistance R_{eff} of the test section.

Reynolds number. A fit using Eq. (1) can then be performed to the data points applying the Gauss–Newton method, where R_{eff} is a free fit parameter, see Fig. 3. All data points are based on equal thermal conditions in a range of $2600 < Re < 10000$ representing exclusively turbulent flow and a mass flux of about 200–1200 kg/m^2 s.

The temperature difference along the sensor support ΔT_{tr} can now be expressed as:

$$\Delta T_{tr} = \dot{Q}_{ts} \cdot R_{eff} \tag{2}$$

Here, $\dot{Q}_{ts}$ is an applied heat flow to the test section, which is determined by precise current and voltage measurement within a maximum error of 1.2%. With consideration of the correction value, the actual circumferential mean heat transfer coefficient is calculated with:

$$\bar{\alpha} = \frac{\dot{Q}_{ts}}{A_{w,i}(\Delta\bar{T}_w - \Delta\bar{T}_{fl} - \Delta\bar{T}_{tr})} \tag{3}$$

The excellent agreement (within a range of ±5%) between predicted and measured single phase heat transfer coefficient is shown in Fig. 4. It confirms reliability and accuracy of the experimental setup. The thermal resistance R_{eff} determined from single phase data can be applied for two-phase flow since R_{eff} is a constant material property of the temperature sensor supports [29].

The maximum error of the heat transfer coefficient calculated in the two phase region is about ±6% at low vapor quality and about ±10% in the dryout region in this study.

The actual vapor quality x, which characterizes the mass fraction of liquid and vapor in the flow, is calculated as follows:

$$x = \frac{h_x - h_l}{h_v - h_l} \tag{4}$$

where h_v and h_l are vapor and liquid saturation enthalpy, respectively. h_x corresponds to the actual enthalpy in the two-phase region and can be calculated as:

$$h_x = h_{start} + \Delta h_{PH} + \Delta h_{ts} = h_{start} + \frac{\dot{Q}_{PH}}{\dot{m}} + \frac{\dot{Q}_{ts}}{2\dot{m}} \tag{5}$$

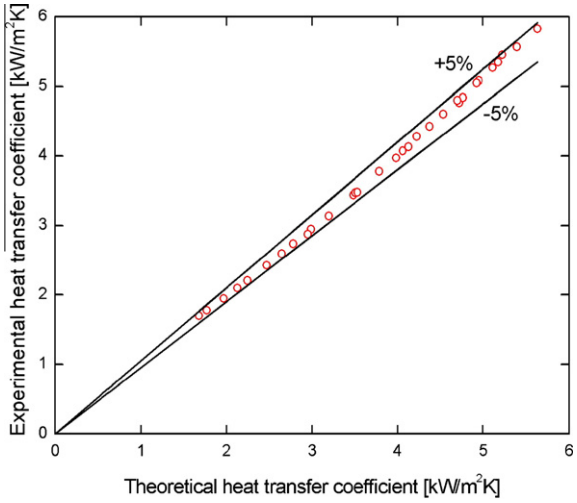

Fig. 4. Theoretical versus experimental single-phase heat transfer coefficient using the model from Gnielinski [28].

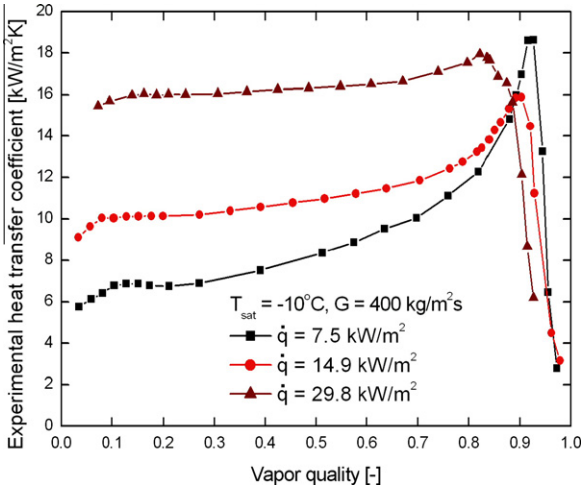

Fig. 5. Mean heat transfer coefficient versus vapor quality, heat flux dependency.

The calibration of the Bronkhorst® F-112AC mass flow meter has been validated in the measured mass flow range with an accuracy of ±2% of reading. The starting enthalpy h_{start} in the two-phase region is defined by the temperature and pressure in the subcooled liquid, where an ideal isenthalpic expansion is assumed. The enthalpy difference Δh_{PH} is created by the heat load $\dot{Q}_{PH}$ to the pre-heater. $\dot{Q}_{PH}$ is varied during the measurement series to adjust to a desired vapor quality to enter the test section. The enthalpy difference Δh_{ts} is calculated at the middle of the test section, see Eq. (5). This assumption will lead to a smoothing effect by calculating the vapor quality, especially at high heat loads and low mass flow rate. The maximum error of the measured mean vapor quality in this study is about ±2%.

A Rosemount® differential pressure sensor is connected with the in- and outlet of the test section to determine the pressure drop, in the range of −300 to 300 mbar with a precision of ±1.5 mbar.

4. Experimental results and discussion

An extensive measurement series has been carried out to characterize the heat transfer coefficient and pressure drop in two-phase flow. A database has been established containing about 2000 measurement points. The effects of various parameters such as mass flux, heat flux and saturation temperature on the heat transfer and pressure drop have been studied. Representative results for each single dependency will be presented and discussed in detail. Unless otherwise defined, all other cases referred to in this paper have similar trends with the parameter dependence.

4.1. Heat flux dependency

Fig. 5 shows the effect of the heat flux $\dot{q}$ on the mean heat transfer coefficient $\bar{\alpha}$ at a saturation temperature of $T_{sat} = -10$ °C and a mass flux of $G = 400$ kg/m^2 s. It can be seen that the heat flux has a significant effect on the heat transfer coefficient. With increasing heat flux, the heat transfer coefficient also increases until the characteristics of the curves equal a plateau at a heat flux of 29.8 kW/m^2. In this case, the heat transfer is in a wide range nearly independent of the vapor quality x. As the critical boiling nuclei radius r_{crit} becomes smaller with an increasing heat flux [30], which will directly influence on the nucleate boiling intensity. Smaller r_{crit} causes more possible boiling nuclei along the tube wall. Hence, the increase of nucleate boiling heat transfer explains the increase of $\bar{\alpha}$ at lower vapor qualities since nucleate boiling is predominant. However in annular flow regime, the convective boiling heat transfer becomes predominant. The convective boiling heat transfer is also enhanced by the higher heat flux due to the more intensive convection in the liquid film. Additionally, a thinner liquid film lowers its effective thermal resistance and enhances the heat transfer. Finally, the more intensive reduction of the liquid film thickness due to higher heat flux yields to the depletion of the liquid film along the tube wall at lower vapor qualities. This explains the earlier onset of dryout with higher heat flux. Dryout of liquid film is determined when the wall temperature rapidly increases and the heat transfer coefficient sharply drops. The trend that the heat transfer increases and the dryout occur earlier with higher heat flux is also observed in [15,31].

The measurement of the pressure drop is performed simultaneously to the heat transfer determination. It can be seen in Fig. 6 that at low vapor quality $x < 0.2$, higher heat flux causes a little higher pressure drop, but at higher vapor qualities the heat flux has an insignificant effect on the two-phase frictional pressure drop even if there is no heat flux at the test section. When a heat flux is applied to the test section the measured pressure drop is the sum of the frictional and the acceleration pressure drop for the horizontal minichannel. Considering that the acceleration pressure drop along the short test section is negligible, the experimen-

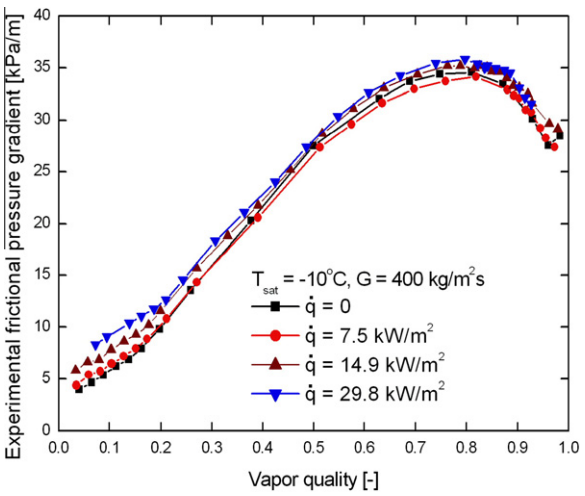

Fig. 6. Frictional pressure gradient versus vapor quality, heat flux dependency.

tal pressure drop discussed in this paper only refers to the frictional pressure drop.

All curves show an increasing pressure drop with increasing vapor quality with a clear maximum vapor quality around $x = 0.8$. During the dryout ($x > 0.8$), the liquid is entrained into the vapor core in form of droplets which are carried by the vapor flow. This transition from annular flow via dryout to mist flow is related to decreasing frictional pressure drop [13]. Compared to the heat transfer coefficient in Fig. 5 there is no sharp pressure drop after onset of dryout.

This observation is consistent with the experimental pressure drop results for different working fluids in different shaped tubes in [32,33].

4.2. Mass flux dependency

The mean heat transfer coefficient versus the vapor quality as function of the mass flux is shown in Fig. 7. For a measurement series the saturation temperature $T_{sat} = -10$ °C as well as the heat flux $\dot{q} = 7.5$ kW/m^2 is kept constant while the mass flux G varies in a range from 300 to 600 kg/m^2 s.

As can be seen in Fig. 7 the mass flux G has no significant influence on the heat transfer coefficient at low vapor qualities. This can be explained by the predominance of the nucleate boiling in the intermittent flow regime.

At vapor qualities $x < 0.2$, the influence on the mass flux G becomes visible. Higher mass flux means higher flow velocity and higher Reynolds numbers, which leads to an enhancement of the vapor as well as of the liquid convective heat transfer. Hence, the convective portion of the heat transfer coefficient becomes higher with a higher vapor quality.

With higher vapor qualities, a sharp increase of the heat transfer coefficient for all mass fluxes can be observed. The reason can still be found in the liquid film thickness at the inner tube wall as mentioned for the heat flux dependency.

It can also be seen in Fig. 8 that at the higher heat flux $\dot{q} = 29.8$ kW/m^2 the heat transfer coefficient does not change considerably with the mass flux variation in a wide range of vapor qualities.

The effect that the onset of dryout occurs at slightly higher vapor qualities for higher mass flux observed by Yun et al. [34] cannot be confirmed from Fig. 7. For a high heat flux, the trend of later dryout with increasing mass flux is visible in Fig. 8. However, this trend is different from data presented in [11,26]. Considering the

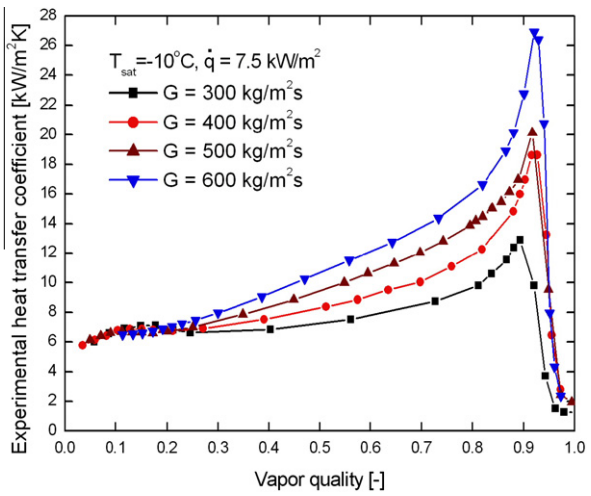

Fig. 7. Mean heat transfer coefficient versus vapor quality, mass flux dependency ($\dot{q} = 7.5$ kW/m^2).

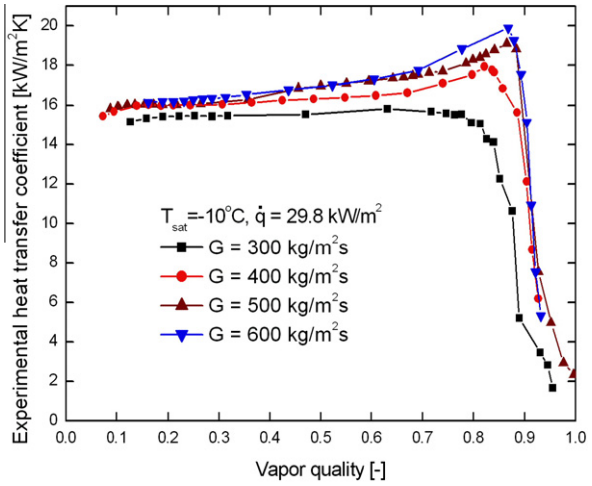

Fig. 8. Mean heat transfer coefficient versus vapor quality, mass flux dependency ($\dot{q} = 29.8$ kW/m^2).

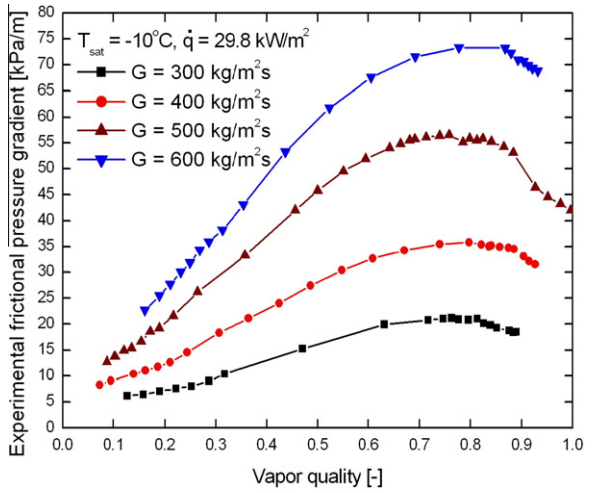

Fig. 9. Frictional pressure gradient versus vapor quality, mass flux dependency.

smoothing effect in determining the vapor quality, the trend seems to be dependent on the chosen measurement procedure.

Fig. 9 shows that the mass flux has a strong effect on the frictional pressure drop. Increasing mass flux results in a higher flow velocity which causes an increase of the frictional pressure drop. This is consisted with research in [35].

4.3. Saturation temperature dependency

Fig. 10 shows the mean heat transfer coefficient plotted versus the vapor quality for different saturation temperatures in the range from −40 to 0 °C (reduced pressures from 0.136 to 0.472). The two-phase flow characteristics of CO_2 evaporation is greatly affected by the high reduced pressure because of the low surface tension and low viscosity, thus the high reduced pressure results in different heat transfer and pressure drop. The mass flux $G = 300$ kg/m^2 s is kept constant while a heat flux $\dot{q} = 7.5$ kW/m^2 is applied to the test section. The experiment shows that higher saturation temperatures lead to higher heat transfer coefficients in the low vapor quality range $x < 0.25$. However, this order changes with increasing vapor quality. There is a local maximum in the heat transfer coefficient curve where the flow regime transition from intermittent flow to annular flow happens. This transition varies in vapor qual-

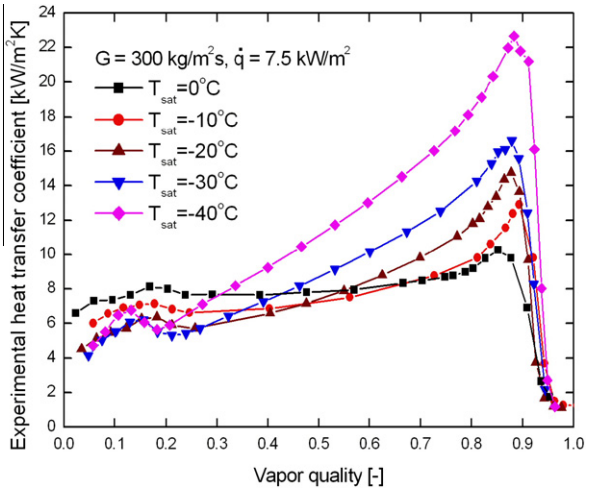

Fig. 10. Mean heat transfer coefficient versus vapor quality, saturation temperature dependency ($\dot{q} = 7.5$ kW/m^2).

ity between 0.1 and 0.2 for different saturation temperatures. The global peak value of the heat transfer coefficient is higher with lower saturation temperature. Lowering the temperature increases the surface tension which is tantamount with a better wetting of the tube wall resulting in a higher heat transfer coefficient before the dryout commences.

It can be seen in Fig. 11 that the heat transfer coefficient becomes almost independent in a wide range of vapor qualities and finally a plateau if a higher heat flux, e.g. $\dot{q} = 29.8$ kW/m^2 is applied to the test section.

This effect of increasing heat transfer coefficient with an increase of saturation temperature at high applied heat flux can be explained by the enhancement of the nucleate boiling due to the decrease of surface tension. This is also observed in [15,36]. The surface tension changes by a factor of more than two in the range between 0 and −40 °C. Decreasing surface tension leads to a decreasing critical radius of the boiling nuclei. The more boiling nuclei exist at the tube wall, the more intensive activation of nucleate boiling takes place. Nucleate boiling is generally predominant at low vapor quality regions. However at moderate quality factors, the nucleate boiling is suppressed and convective heat transfer becomes predominant caused by higher vapor flow velocities with lower saturation temperatures, which explains well the effect of the order variation. The ratio of vapor and liquid density is a measure of the relation between liquid and vapor flow velocity [37]. The flow velocity ratio ω_l/ω_v becomes smaller with a decrease of saturation temperature which causes an enhancement of the convective heat transfer coefficient. According to [38] the onset of dryout is supposed to occur at slightly lower vapor quality with decreasing surface tension. The experimental trend of the onset of dryout is not substantiated by this study. Fig. 12 shows the two-phase frictional pressure drop at different saturation temperatures in a range of −40 to 0 °C. As the saturation temperature decreases (at constant mass flux and heat flux condition), the increasing liquid density results in a lower liquid velocity. Contrary, decreasing vapor density results in a higher vapor velocity. Higher vapor velocity and lower liquid velocity cause higher frictional pressure drop. Furthermore, a higher saturation temperature may cause a higher liquid depletion and then cause dryout to occur earlier, although this trend is not obvious in Fig. 12.

5. Comparisons with the prediction model

A general flow pattern map based on flow boiling heat transfer model has been developed for CO_2 by Cheng et al. [1,2]. The model

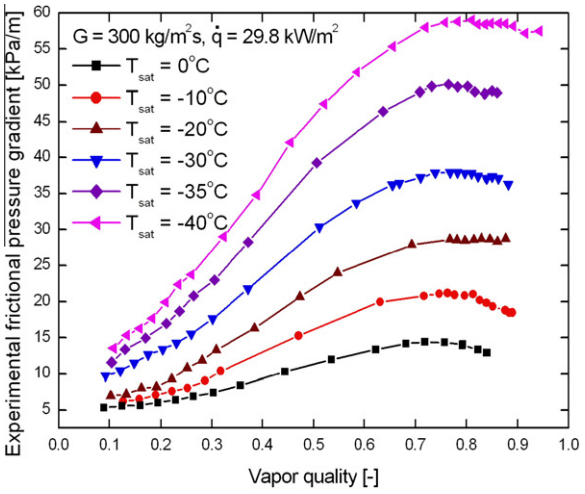

Fig. 12. Frictional pressure gradient versus vapor quality, saturation temperature dependency.

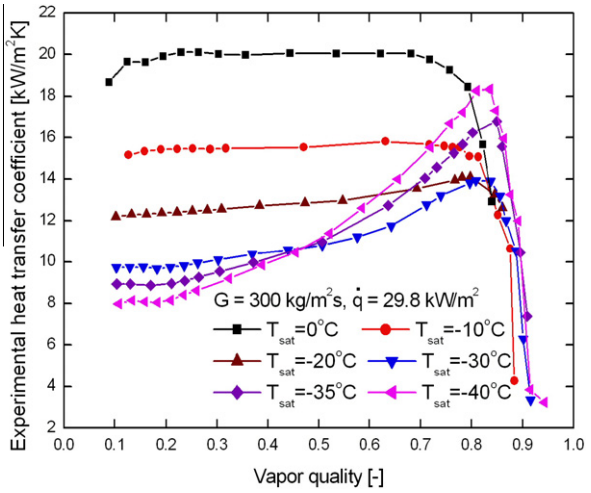

Fig. 11. Mean heat transfer coefficient versus vapor quality, saturation temperatures dependency ($\dot{q} = 29.8$ kW/m^2).

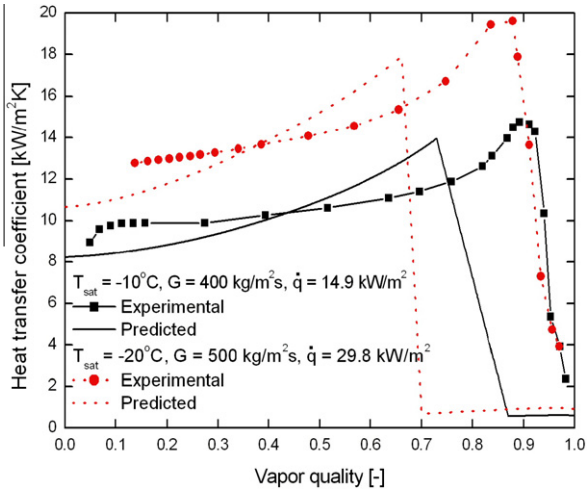

Fig. 13. Comparison of the experimental data with the prediction model developed by Cheng et al. [2]. Two typical heat transfer dependencies are chosen exemplarily.

covers all flow regimes and is applicable to a wide range of conditions including the experimental conditions present in this paper.

Fig. 13 exemplarily shows the comparisons between the heat transfer coefficients predicted by the model and the presented experimental data sets including the dependencies of heat flux, mass flux and saturation temperature. According to the figure, the overall heat transfer trends and the experimental heat transfer data are well predicted by the model. However the onset of dryout (peak) is predicted to start at lower vapor quality for all the presented experimental results.

Actually measurement of heat transfer data in the dryout and mist flow regimes is substantially difficult. Additionally, the overall scanning in the two-phase region is too rough to determine the exact onset of dryout. Nevertheless, there is a very reliable procedure to evaluate the onset of dryout by recording the temperature evolution during the scanning of the two-phase region.

Fig. 14 shows an example of temperature evolution at the test section during the whole scanning process. At $x = 0.08$, for a respective heat input into the heated part of the test section, the wall temperatures increase while the fluid temperatures remain constant. When the vapor quality reaches 0.78 by increasing the heat input into the pre-heater, the wall temperature T_{w3} starts oscillating which indicates the onset of dryout. The average value of T_{w3} is still decreasing which leads to an increase of heat transfer coefficient. Due to the averaging of three wall temperature, the onset of dryout only becomes visible at a notably increase of T_{w3} at a higher vapor quality $x = 0.85$.

Because the two-phase frictional pressure drop is measured directly by the differential pressure sensor, it is much more reasonable to evaluate the flow characteristics using the experimental pressure drop results. Fig. 15 shows the experimental data at $T_{sat} = -10\ ^{\circ}C$, $G = 400\ kg/m^2\ s$ and $\dot{q} = 14.9\ kW/m^2$ as an example corresponding to a flow pattern map developed by Cheng et al. [1] at the same conditions. Area I refers to intermittent flow, A to annular flow, D to dryout region and M to mist flow. It can be seen that the pressure drop reaches a relative stable peak region in the dryout regime. Then the pressure drop starts decreasing after the flow becomes a mist flow. Therefore, the point of onset of dryout, which is determined by the pressure drop measurement, matches with the predicted model.

However, due to the very few and less accurate experimental data in minichannels in the literature, the CO_2 two-phase flow pressure drop model does not satisfactorily predict the experimental data in this study at high vapor qualities and in mist flow. Seen the large number of experimental CO_2 pressure drop data, obtained

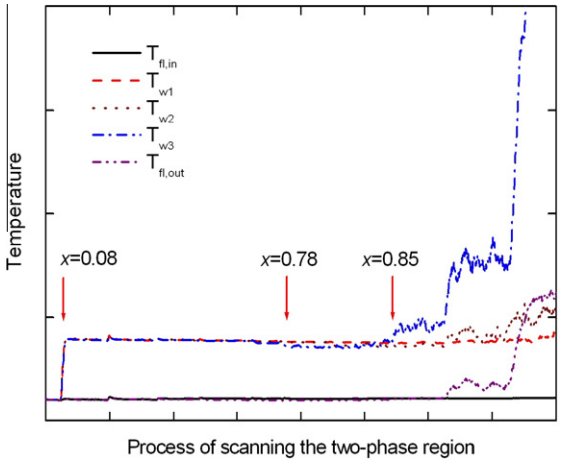

Fig. 14. Time evolution of the temperature at the test section in the whole two-phase region scanning process.

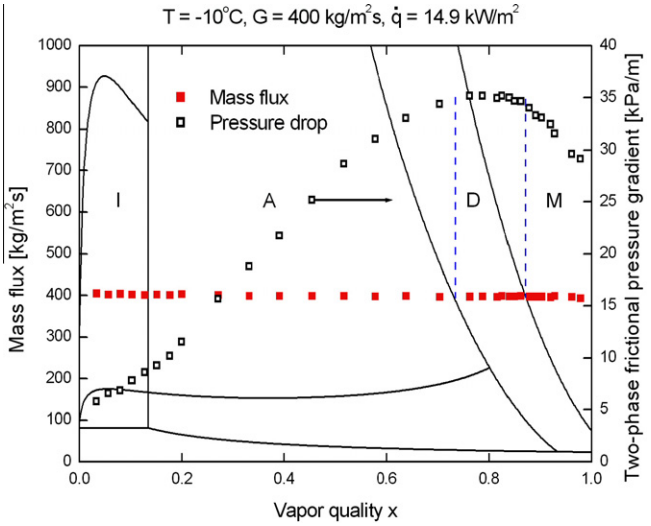

Fig. 15. Comparison of the experimental pressure gradient data in the flow pattern map. The dashed lines indicate the vapor quality of the onset of dryout and the beginning of the mist flow regime.

in mist flow during this study, the modification of the model is only made to the mist flow frictional factor expression. As a result, the predicted pressure drop in the dryout region is also modified because the linear interpolation expression between annular and mist flow is kept the same as in [1]. Compared to the pressure drop model, which overpredicts the pressure drop in mist flow regime, the modified correlation is proposed as:

$$f_m = \frac{2.214}{Re^{0.521}} \tag{6}$$

Fig. 16 shows the comparison of the pressure drop model including the modification in mist flow with the experimental data. It can be seen that the model predicts the overall trend up to moderate vapor qualities in the annular flow regime. In the vapor quality range from 0.6 to 0.8, the experimental data show smooth transition from the annular to the mist flow regime via the dryout instead of the peak calculated by the prediction model (dotted line).

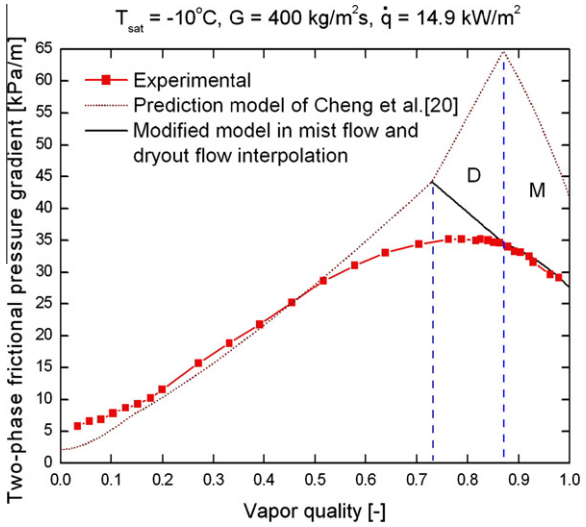

Fig. 16. Comparison of the experimental data with the CO_2 pressure drop model using the modified correlation in mist flow following Eq. (6). The dashed lines indicate the vapor quality of the onset of dryout and the beginning of the mist flow regime.

The new friction factor for the mist flow also works well for macroscale channels and can predict rather similar values for the same experimental conditions [35] mentioned in [1]. For future research, the annular flow friction factor in the model also needs to be modified based on the obtained experimental CO_2 pressure drop database in annular flow.

6. Conclusions

A series of measurement has been carried out to characterize the heat transfer and frictional pressure drop phenomena of CO_2 two-phase flow in a horizontal circular tube with a diameter of 1.42 mm. The reliability and accuracy of an experimental setup has been confirmed by the good agreement between predicted and measured CO_2 single phase heat transfer coefficient within a range of ±5%. The dependencies of heat flux $\dot{q}$ in the range from 7.5 to 29.8 kW/m^2, mass flux G from 300 to 600 kg/m^2 s and saturation temperature T_{sat} between 0 and −40 °C have been investigated. A database has been established containing about 2000 measurement points. The following conclusions can be obtained:

(1) It has been observed that at low vapor qualities nucleate boiling is predominant and strongly dependent on the heat flux $\dot{q}$ and the saturation temperature T_{sat}. Higher heat flux and higher saturation temperature lead to an enhancement of nucleate boiling caused by an increasing activation of boiling nuclei along the tube wall. At moderate quality factors, representing the annular flow regime, nucleate boiling is suppressed with increase of vapor quality. The mass flux G influences the flow velocity and hence the Reynolds number. High flow velocity increases the convective heat transfer which is dominant for small heat fluxes or at high vapor qualities. Higher saturation temperature enhances nucleate boiling due to smaller surface tension. Lower saturation temperature on the other hand increases the convective heat transfer due to the higher ratio of vapor and liquid velocity. Generally the heat flux shows the strongest influence on the flow boiling heat transfer for all the presented results.
(2) The onset of dryout (peak) is predicted by the model of Cheng et al. [2] to start at lower vapor quality compared to the presented experimental data. The reason for this difference can be explained by the determination of the onset of dryout during the scanning process of the two-phase region.
(3) The maximum experimental frictional pressure drop is determined in the dryout region which derives from the flow partner map [1,2].
(4) Heat flux has insignificant effect on two-phase frictional pressure drop. The measured pressure drop increases as mass flux increases (caused by increasing flow velocity) and as saturation temperature decreases (caused by the variation of thermophysical properties).
(5) A modified friction factor in mist flow based on the experimental data has been proposed. The modified model of the two-phase flow frictional pressure drop predicts the experimental data well for all flow regimes.

Acknowledgements

The authors are indebted to L. Dufay-Chanat, D. Cochet, S. Prunet, J.M. Quetsch, C. Balle, J.L. Servais, H. Pereira and S. Devidal in the Cryolab at CERN for the support, advice and technical help in this study. The discussions and constructive suggestions during the course of these investigations by Prof. John R. Thome of the Laboratory of Heat and Mass Transfer (LTCM) at Ecole Polytechnique Fédérale de Lausanne (EPFL) are greatly acknowledged. The authors would like to express deep gratitude to Hans Postema and Paolo Petagna both from CERN for their friendly and excellent collaboration.

References

[1] L. Cheng, G. Ribatski, J. Moreno Quibén, J.R. Thome, New prediction methods for CO_2 evaporation inside tubes: Part I – a two-phase flow pattern map and a flow pattern based phenomenological model for two-phase flow frictional pressure drops, Int. J. Heat Mass Transfer 51 (2008) 111–124.
[2] L. Cheng, G. Ribatski, J.R. Thome, New prediction methods for CO_2 evaporation inside tubes: Part II – an updated general flow boiling heat transfer model based on flow patterns, Int. J. Heat Mass Transfer 51 (2008) 125–135.
[3] D. Froidevaux, P. Sphicas, General-purpose detectors for the large hadron collider, Annu. Rev. Nucl. Part. Sci. 56 (2006) 375–440.
[4] Michelangelo L. Mangano, The Super-LHC, Report Number: CERN-PH-TH/2009-164, 2009.
[5] The Compact Muon Solenoid Experiment. Available from: <www.cms.web.cern.ch/cms/>.
[6] CERN PH-CMX, PH-DT, TE-CRG groups: R&D work package on development and testing of CO_2 cooling for the LHC tracker upgrades-Pilot case: CMS Pixel detector, EDMS id 925221, 2008, Unpublished results.
[7] K. Klocker, E.L. Schmidt, F. Steimle, Carbon dioxide as a working fluid in drying heat pumps, Int. J. Refrig. 24 (2001) 100–107.
[8] P. Neksa, CO_2 heat pump systems, Int. J. Refrig. 25 (2002) 421–427.
[9] B. Verlaat et al., Feasibility demonstration of a mechanically pumped two-phase CO_2 cooling loop for the AMS-2 tracker experiment, in: Conference on Thermophysics in Microgravity, in the Space Technology & Applications International Forum (STAIF-2002), Albuquerque, NM, USA, 2002.
[10] The LHCb Collaboration, The LHCb VELO Technical Design Report, CERN/LHCC Note, 2001–0011, 2001.
[11] Lixin Cheng, John R. Thome, Cooling of microprocessors using flow boiling of CO_2 in a micro-evaporator: preliminary analysis and performance comparison, Appl. Therm. Eng. 29 (11–12) (2009) 2426–2432.
[12] J. Pettersen, Heat transfer and pressure drop characteristics of evaporating carbon dioxide in microchannel tubes, in: Natural working fluids, Proceedings of the 4th IIR-Gustav Lorentzen Conference on Natural Working Fluids, Purdue University, USA, 2000, pp. 324–334.
[13] R. Yun, Y. Kim, Two-phase pressure drop of CO_2 in mini tubes and micro channels, Microscale Therm. Eng. 8 (2004) 259–270.
[14] R. Yun, Y. Kim, M.S. Kim, Flow boiling heat transfer of carbon dioxide in horizontal mini tubes, Int. J. Heat Fluid Flow 26 (2005) 801–809.
[15] Kwang-Il Choi, A.S. Pamitran, Jong-Taek Oh, Two-phase flow heat transfer of CO_2 vaporization in smooth horizontal minichannels, Int. J. Refrig. 30 (2007) 767–777.
[16] Kwang-Il Choi, A.S. Pamitran, Chun-young Oh, Jong-Taek Oh, Boiling heat transfer of R-22, R-134a and CO_2 in horizontal smooth minichannels, Int. J. Refrig. 30 (2007) 1336–1346.
[17] A.S. Pamitran, Kwang-Il Choi, Jong-Taek Oh, Hoo-Kyu Oh, Two-phase pressure drop during CO_2 vaporization in horizontal smooth minichannels, Int. J. Refrig. 31 (2008) 1375–1383.
[18] Y. Zhao, M. Molki, M.M. Ohadi, S.V. Dessiatoun, Flow boiling of CO_2 in microchannels, ASHRAE Trans. DA-00-2-1 (2000) 437–445.
[19] M.M. Shah, Chart correlation for saturated boiling heat transfer: equations and further study, ASHRAE Trans. 88 (1982) 185–196.
[20] K.E. Gungor, R.H.S. Winterton, A general correlation for flow boiling in tubes and annuli, Int. J. Heat Mass Transfer 29 (1986) 351–358.
[21] Z. Liu, R.H.S. Winterton, A general correlation for saturated and subcooled flow boiling in tubes and annuli based on a nucleate pool boiling equation, Int. J. Heat Mass Transfer 34 (1991) 2759–2766.
[22] L. Friedel, Improved friction drop correlations for horizontal and vertical two-phase pipe flow, in: European Two-phase Flow Group Meeting, Ispra, Italy, 1979, p. E2.
[23] H. Mueller-Steinhagen, K. Heck, A simple friction pressure drop correlation for two-phase flow in pipes, Chem. Eng. Process 20 (1986) 297–308.
[24] S.H. Yoon, E.S. Cho, Y.W. Hwang, M.S. Kim, K. Min, Y. Kim, Characteristics of evaporative heat transfer and pressure drop of carbon dioxide and correlation development, Int. J. Refrig. 27 (2004) 111–119.
[25] L. Cheng, G. Ribatski, J.R. Thome, Gas–liquid two-phase flow patterns and flow pattern maps: fundamentals and applications, ASME Appl. Mech. Rev. 61 (2008) 1–28. 050802.
[26] L. Cheng, G. Ribatski, L. Wojtan, J.R. Thome, Erratum to: "New flow boiling heat transfer model and flow pattern map for carbon dioxide evaporating inside tubes" [Heat Mass Transfer 49 (21–22) (2006) 4082–4094], Int. J. Heat Mass Transfer 50 (2007) 391.
[27] J. Huhn, N. Elsner, S. Fische, Grundlagen der Technischen Thermodynamik, eighth ed., vol. 2, Akademie Verlag, 1993.
[28] V. Gnielinski, Neue Gleichungen für den Wärme- und den Stoffübergang in turbulent durchströmten Rohren und Kanälen, Forsch. im Ing.-Wes. 41 (1975) 8–16.
[29] S. Grohmann, Distributed Cooling in Cryogenics with Miniaturized Fluid Circuits, PhD thesis, Technical University of Dresden, 2004.
[30] VDI-Gesellschaft Verfahrenstechnik und Chemieingenieurwesen, tenth ed., VDI-Wäremeatlas, Springer, 2006.

[31] J. Pettersen, Flow vaporization of CO_2 in microchannel tubes, Exp. Therm. Fluid Sci. 28 (2004) 111–121.
[32] Jesús Moreno Quibén, Lixin Cheng, Ricardo J. da Silva Lima, R. John Thome, Flow boiling in horizontal flattened tubes: Part I – two-phase frictional pressure drop results and model, Int. J. Heat Mass Transfer 52 (2009) 3634–3644.
[33] J. Moreno Quibén, J.R. Thome, Flow pattern based two-phase frictional pressure drop model for horizontal tubes, Part II: new phenomenological model, Int. J. Heat Fluid Flow 28 (2007) 1060–1072.
[34] R. Yun, Y. Kim, M.S. Kim, Two-phase flow patterns of CO_2 in a narrow rectangular channel, in: 21st IIR International Congress of Refrigeration, Washington, DC, USA, 2003.
[35] A. Bredesen, A. Hafner, J. Pettersen, P. Neksa, K. Aflekt, Heat transfer and pressure drop for in-tube evaporation of CO_2, in: Proceedings of the International Conference on Heat Transfer Issues in Natural Refrigerants, University of Maryland, USA, 1997, pp. 1–15.
[36] M. Kim, R. Yun, Y. Kim, Convective boiling heat transfer characteristics of CO_2 in microchannels, Int. J. Heat Mass Transfer 48 (2005) 235–242.
[37] D. Steiner, Zweiphasenströmung in apparateelementen, Forschungs-Gesellschaft Verfahrens-Technik e.V., 1983.
[38] J. Thome, L. Wojtan, T. Ursenbacher, Investigation of flow boiling in horizontal tubes: Part 1 – a new adiabatic two-phase flow pattern map, Int. J. Heat Mass Transfer 48 (2005) 2955–2969.